Letter

Nonlocal thermoelectric detection of interaction and correlations in edge states

Alessandro Braggio,[1] Matteo Carrega,[2] Björn Sothmann,[3] and Rafael Sánchez[4]
[1]*NEST, Istituto Nanoscienze-CNR and Scuola Normale Superiore, Piazza San Silvestro 12, I-56127 Pisa, Italy*
[2]*SPIN-CNR, Via Dodecaneso 33, 16146 Genova, Italy*
[3]*Theoretische Physik, Universität Duisburg-Essen and CENIDE, D-47048 Duisburg, Germany*
[4]*Departamento de Física Teórica de la Materia Condensada, Condensed Matter Physics Center (IFIMAC), and Instituto Nicolás Cabrera, Universidad Autónoma de Madrid, 28049 Madrid, Spain*

(Received 21 July 2023; revised 11 October 2023; accepted 18 January 2024; published 4 March 2024)

Nonlocal thermoelectricity is proposed as a direct probe of interactions, nonthermal states, and the effect of correlations in the nonequilibrium heat transport between 1D quantum channels. In copropagating quantum Hall edge states contacted at different temperatures, the nonlocal thermoelectrical response is *only* expected if the electron-electron interaction mediates the heat exchange directly measuring the interaction strength. Considering the low-energy limit of zero-range interactions, we analytically solve the charge and energy currents of a nonequilibrium interacting system, determining the universal scaling law in terms of an interaction-dependent energy-relaxation length. Further, a setup with two controllable quantum point contacts allows thermoelectricity to monitor the thermalization of an interacting system as well as the fundamental role of cross-correlations in the heat exchange at intermediate length scales.

DOI: 10.1103/PhysRevResearch.6.L012049

Introduction. The thermoelectric response of nanosystems [1] provides a unique tool to probe quantum phenomena such as electron entanglement [2–4], superconducting [5–7] and topological properties [8–12], entropy [13], photon-assisted tunneling [14], or the chirality of quantum Hall (QH) states [15–17]. The direct conversion of temperature differences into measurable electrical quantities enables the exploration of heat exchange in quantum-coherent systems far from equilibrium [18,19]. Multiterminal configurations allow for a separation of heat-injecting and charge-propagating channels [20–22].

Copropagating QH edge channels (ECs) can be contacted electrically separately [23,24], thus allowing for precise electrical manipulation. Electron-electron (e-e) interactions have been investigated via the energy relaxation from nonthermal and non-Gaussian states injected either by a quantum point contact (QPC) [25] or as hot electrons [26,27]. However, their detection is challenging [28–34] and the results difficult to analyze [35–37]. Moreover, thermal probes have been used to measure quantized thermal conductances with edge states [38], to address the nature of edge states [39–43], to explore equilibration mechanisms [44,45] and to image thermal decay [46,47]. In this Letter, we suggest the nonlocal thermoelectric QH effect to probe nonequilibrium heat exchange mediated by e-e interaction in one dimensional (1D) electron gases, which can be computed analytically. A thermocurrent is generated when an energy-dependent junction connects terminals at different temperatures [17]. Hereafter, the hot terminal at temperature T_+ injects electrons into the inner channel, while the outer channel connects with transmission probability $\mathcal{T}(E)$ two terminals with identical temperatures $T_- < T_+$ (see Fig. 1). When all terminals are grounded, the nonlocal thermoelectric response of the two separate channels is hence zero, unless they exchange heat via Coulomb interactions [48,49]. Then a thermocurrent

$$I = -\int dE\mathcal{T}(E)[f_{eq}(E,T_-) - f_-(x,E)], \tag{1}$$

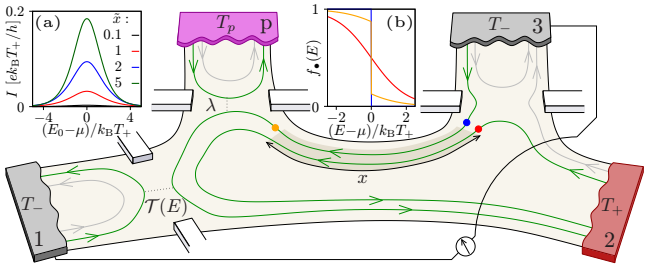

FIG. 1. QH detection setup. The interaction of the upper ECs along the distance x before a scatterer of transmission probability $\mathcal{T}(E)$ enables a thermoelectric response between terminals 1 and 3, both at temperature T_-, when terminal 2 injects into the inner channel electrons at a temperature $T_+ \neq T_-$. Inset (a) shows the thermoelectric current for interacting regions of different lengths $\tilde{x} = x/x_K^+$ with $x_K^+ = \hbar v_F/[\pi(1-K)k_BT_+]$ and $T_- = 0.5T_+$, when $\mathcal{T}(E) = \Theta(E-E_0)$ (e.g., a QPC), and (b) the distribution of the different channels before [in red (+) and blue (−)] and after [orange (−)] the interacting region, as indicated by coloured dots on the main scheme, with $x = 2x_K^+$ and $T_- = 10^{-3}T_+$. The coupling λ to a probe terminal p can be used to inject thermalized electrons.

Published by the American Physical Society under the terms of the Creative Commons Attribution 4.0 International license. Further distribution of this work must maintain attribution to the author(s) and the published article's title, journal citation, and DOI.

between terminals 1 and 3 pinpoints the presence of e-e interactions in the region of length x (we set $e = \hbar = k_B = 1$). The thermocurrent depends on the difference between the nonequilibrium distribution of the outer channel $f_-(x, E)$ after the interacting region, and the equilibrium Fermi distribution $f_{eq}(E, T_-)$ of terminal 1 [50,51]. The longer x, the larger the generated current, see Fig. 1(a) for the case of a QPC scatterer, as expected. The deviation of $f_-(x, E)$ [plotted in Fig. 1(b)] from an equilibrium distribution can be interpreted as an overheating effect that can be eventually compared with the equilibrium distribution of a probe with an effective temperature T_p. We describe how 1D electronic channels initially at different temperatures restore thermal equilibrium through e-e interactions using the nonlocal thermoelectric response as a detector. The analysis is done in the zero-range interaction limit, valid in the low-energy regime with integrable physics. Our device uses the chiral nature of ECs to convert the time evolution into a space evolution, allowing us to identify the interaction-dependent length scale over which Tomonaga-Luttinger (TL) liquids [52,53] relax thermal gradients. Finally, we use the thermoelectric signature to underline the role of the cross-correlations in thermal relaxation.

Interacting channels. We consider copropagating edge states of a QH fluid filling the lowest Landau level [36] at ν=2, which interact long enough to reveal the e-e interactions [24]. Using bosonization [54,55], 1D ECs can be described in terms of bosonic phase fields $\phi_\pm(x', t)$. Assuming that zero-range e-e interactions between the two channels ($\alpha, \beta = \pm$) are restricted to a finite region of length x, the equations of motion (EoM) for $0 \leqslant x' \leqslant x$ become $\partial_t \phi_\alpha + \sum_\beta v_F u_{\alpha\beta} \partial_{x'} \phi_\beta = 0$, where v_F is the Fermi velocity. The density-density zero-range interaction, $u_{\alpha\beta} = \delta_{\alpha\beta}(1 + u_4) + (1 - \delta_{\alpha\beta})u_2$, describes intra- ($u_4$) or inter- ($u_2$) channel terms [24,56]. Using the current operators at $x = 0$, $\hat{J}_\alpha(t) \equiv -\partial_t \phi_\alpha(0, t)/(2\pi)$, as boundary conditions [25,55], the EoM are analytically solved by introducing charge and dipole modes $\phi_{c/n}(x, t) = [\phi_+(x, t) \pm \phi_-(x, t)]/\sqrt{2}$, chiral copropagating fields with velocities $v_{c/n} = v_F(1 + u_4 \pm u_2)$. We assume $u_4 = u_2$, so $v_n = v_c K = v_F$ with $K \equiv 1/(1 + u_4 + u_2)$ [57]. The normal modes chirality, $\phi_\sigma(x, t) = \phi_\sigma(0, t - t_\sigma^x)$ with $t_\sigma^x = x/v_\sigma$ and σ = c,n connects the phase-field operators with the boundary conditions such that the channel current operators $j_\pm(x, \omega) = \frac{1}{2}\sum_{\alpha=\pm}(e^{i\omega t_c^x} \pm \alpha e^{i\omega t_n^x})\hat{J}_\alpha(\omega)$. We used the linearity of the theory with the Fourier representation $f(\omega) = \int dt e^{i\omega t} f(t)$. Correlations between the two EC induced by e-e interactions at a given position x can be inspected by looking at the noise spectral density, $S_x^{\alpha\beta}(\omega) = \delta(\omega + \omega')\langle j_\alpha(x, \omega) j_\beta(x, \omega')\rangle$. Note that the δ function in the right-hand side is due to the linearity of the theory stating that bosonic modes at different energies are independent quantities. In general, e-e interactions influence both finite auto- $S_{x'}^{\alpha\alpha}(\omega)$ and cross-correlations $S_{x'}^{\alpha\beta}(\omega)$ (with $\alpha \neq \beta$) at any point x', which can be expressed in terms of the boundary correlators $S_0^{\alpha\beta}(\omega) = \langle \hat{J}_\alpha(\omega)\hat{J}_\beta(-\omega)\rangle$,

$$
\begin{aligned}
S_x^{\alpha\alpha}(\omega) &= \bar{S}_0^{\alpha\alpha}(\omega) + \frac{\cos(\omega\delta t^x)}{2}\delta S_0^{\alpha\alpha}(\omega), \\
S_x^{\alpha\bar{\alpha}}(\omega) &= -\frac{i}{2}\sin(\omega\delta t^x)\delta S_0^{\alpha\alpha}(\omega),
\end{aligned}
\tag{2}
$$

where $\bar{S}_x^{\alpha\beta}(\omega) \equiv (S_x^{\alpha\beta} + S_x^{\bar{\alpha}\bar{\beta}})/2$, $\delta S_x^{\alpha\beta} \equiv S_x^{\alpha\beta} - S_x^{\bar{\alpha}\bar{\beta}}$, with $\bar{\alpha} = -\alpha$, and where $\delta t^x = t_n^x - t_c^x = x(1 - K)/v_F$ depends on the interaction strength $0 < K \leqslant 1$. The unsymmetrized (emission) noise spectral density for the noninteracting leads at temperature T_α is $S_0^{\alpha\alpha}(\omega) = \omega[1 - e^{-\omega/T_\alpha}]^{-1}e^{-\omega/\omega_c}$, with the high-energy cut-off ω_c [25]. However, finite cross-correlations $S_x^{\alpha\bar{\alpha}}(\omega)$ develop due to e-e interactions, see Eq. (2), which are absent for independent channels. Notably the cross-correlators satisfy the symmetry $S_x^{\alpha\bar{\alpha}}(\omega) = S_x^{\bar{\alpha}\alpha}(\omega)^*$ and are finite only when $S_0^{++}(\omega) \neq S_0^{--}(\omega)$, such as in nonequilibrium for $T_+ \neq T_-$. The correlation effects and the oscillating behavior with x or ω in Eq. (2) are potentially measurable and are a signature of a nonequilibrium situation *with* the presence of e-e interactions $K < 1$ (see the Supplemental Material (SM) [58]). Further, the oscillating period in position (frequency) for fixed frequency (position) measures the interaction strength. In the following, we show two different configurations in which the role of auto and cross-correlations, and the effects of e-e interactions, can be directly probed by the thermoelectrical response. This model is realistic for experimental realizations [24] operating at sub-Kelvin temperatures as usually realized for recent QH thermal experiments [15,16,38,42]. For $T_+ \approx 500$ mK and $T_- \approx 250$ mK we expect a measurable thermoelectric current of a few nA with $x_K^+ \approx 500\text{nm}/(1 - K)$ for $v_F \approx 10^5$m/s, much smaller that the typical length where disorder effect appears [49].

Energy exchange and effective temperature. When the two channels are out-of-equilibrium, such that $T_+ \neq T_-$, it is interesting to investigate how the energy transfer J_E between the two EC depends on the interaction K and the length x of the interacting zone. Since direct energy exchange measurements are challenging, here we propose to use nonlocal thermoelectricity to measure the EC heat transfer. In particular, we assume that, using QPCs, we can completely separate the ECs after the interaction and analyze them separately (see the SM [58]). In the limit of a long interacting zone $x \to \infty$, the energy exchanged becomes independent of distance and interaction strength $J_E \propto T_+^2 - T_-^2$. This is consistent with the expectation that after a long distance, the two interacting ECs equilibrate towards the equilibrium temperature $T^{\text{eq}} = \sqrt{T_-^2 + T_+^2}$ reached by two Fermi liquids with different temperatures put in contact. For an isolated EC for $x' > x$, one can similarly define an effective temperature $T_\pm^{\text{eff}}(x') = \sqrt{T_\pm^2 \mp \frac{12}{\pi} J_E(x')}$, which corresponds to the temperature of a Fermi liquid thermalized with the EC even for non-Fermi liquid electronic distributions (see the SM [58]). For the ECs we find

$$
\frac{T_\pm^{\text{eff}}(x)}{T_+} = \sqrt{\frac{1}{2} \mp \frac{3/2}{\sinh^2 \tilde{x}} + \frac{\varrho^2}{2}\left[1 \pm \frac{3}{\sinh^2(\varrho\tilde{x})}\right]}, \tag{3}
$$

where $\tilde{x} \equiv x/x_K^+$ is the rescaled interacting length, and $\varrho \equiv T_-/T_+$ represents the initial temperature unbalance between the channels. The interaction-dependent effective length $x_K^+ = \hbar v_F/[\pi(1-K)k_B T_+]$ is the typical distance over which the exchange of energy happens between the hot T_+ and the cold ($T_- \to 0$) channels. In Fig. 2 we show the scaling of $T_\pm^{\text{eff}}$ as a function of $\tilde{x}$ for different ratios ϱ. Increasing the interaction length $x \gg x_K^+$ the effective temperature equilibrates to the

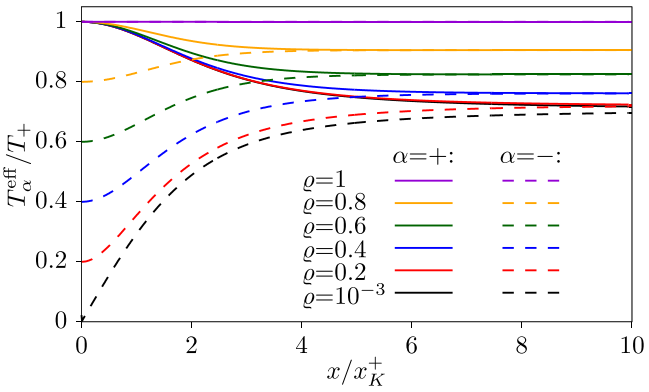

FIG. 2. Effective temperature $T_\alpha^{\rm eff}/T_+$ of the $\alpha=\pm$ channels vs the rescaled position x/x_K^+ for different $\varrho = T_-/T_+$.

intermediate value of Fermi liquids, $T^{\rm eq}/T_+ = \sqrt{(1+\varrho^2)/2}$. In the limit $\varrho \to 0$, Eq. (3) tends to a universal curve leading to a universal formula for the thermal conductance $G_{th}(x) \approx J_E(x)/\delta T$ assuming initially a small temperature difference δT between the ECs (see the SM [58]). Note that the x dependence can be explored by modifying the length of the QH edges using electrostatic gates [59]. Alternatively, one can fix x and change T_+.

Circuit theory for correlators. The presence of e-e interactions and nonequilibrium can generate finite cross-correlations between the ECs. In particular, using the locality (due to zero-range assumption) and linearity of the theory (see the SM [58]) we can write any correlator $S^{\alpha\beta}_{y+x}(\omega)$ as a chain rule via correlators $S^{\alpha\beta}_x(\omega)$ at intermediate position x,

$$S^{\alpha\beta}_{y+x}(\omega) = \bar{S}^{\alpha\beta}_x + \frac{\cos(\omega\delta t^y)}{2}\delta S^{\alpha\beta}_x + i\frac{\sin(\omega\delta t^y)}{2}\delta S^{\alpha\bar{\beta}}_x, \quad (4)$$

with the symmetric and antisymmetric combinations of boundary condition spectral densities. This generalizes Eq. (2) to nonequilibrium situations and potentially non-Gaussian boundary conditions. However, the chain rule is still valid to *effectively* describe a region with long-range interaction between ECs, as long as the correlators are analyzed in zero-range interacting regions. This assumption is not particularly demanding: indeed usually, two edge channels need to be separated by gating [23] (with e.g., a QPC) to contact them separately and, in such cases, the zero-range assumption is typically recovered due to screening effects. The correlators $S^{\alpha\beta}_x(\omega)$ in a zero-range region contain all the required information about averaged quantities (e.g., charge/energy currents) and the noise fluctuations (e.g., second-order current-current correlators) in the system. This is a sort of *generalized* nonequilibrium circuit theory. One could easily combine regions with different strengths of interactions. In Eq. (4) the influence cross(auto)-correlators on the later-time auto(cross)-correlators appears via the term proportional to $i\sin(\omega\delta t^y)$. This shows that the cross-correlations generated in an interacting system out-of-equilibrium *cannot* be ignored to investigate the energy flow. Below we introduce an experimental setup able to eventually switch on and off the cross-correlation contributions in a controlled way.

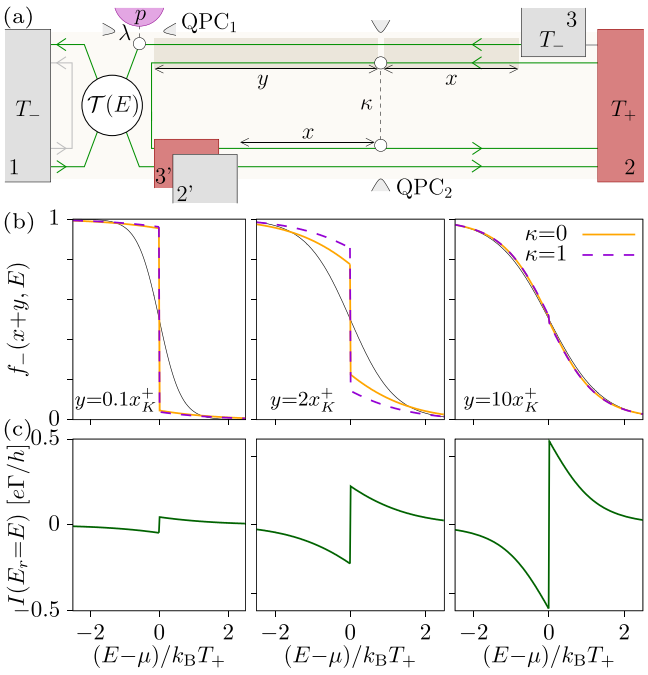

FIG. 3. (a) Nonequilibrium- and cross-correlation-sensitive circuit. Channels at the upper and lower edge are uncoupled for $\kappa=0$. Switching on the connection $\kappa=1$, inner electrons from terminal 2 are replaced by others from 2'. (b) Nonequilibrium electron distribution function for the cold EC as a function of energy E/T_+ for different cases: fully interacting ($\kappa = 0$), and with cross-correlation resetting ($\kappa = 1$), compared with the equilibrium Fermi distribution with temperature $T_-^{\rm eff}(y+x)$ (black). Different panels refer to different positions y/x_K^+, with $\varrho=10^{-3}$. (c) Current for the correspondingly above cases ($\kappa = 0$) when the scatterer is a narrow resonance, $\mathcal{T}(E) \approx \Gamma\delta(E-E_r)$.

Nonequilibrium electron distributions. The fundamental quantity in ECs is the electron distribution function $f_\alpha(y+x,t) \equiv \langle\psi^\dagger_\alpha(y+x,t)\psi_\alpha(y+x,0)\rangle$ where, in bosonization, the operators are expressed in terms of phase fields since $\psi_\alpha(x,t) \propto e^{-i\phi_\alpha(x,t)}$. However, in order to address the role of cross-correlations in the energy exchange mediated by the interaction we investigate the thermoelectricity in a specific setup, see Fig. 3(a). We consider two EC separately contacted with Ohmic contacts at different temperatures T_α at $x<0$. They start to interact from $x \geqslant 0$, and we measure the thermoelectric response induced by the outer EC at the scatterer $\mathcal{T}(E)$ located at $y+x>0$. At an intermediate position x one can imagine to selectively open, $\kappa=1$, (close, $\kappa=0$) the $\rm QPC_2$, switching on (off) the cross-correlation [60].

The real-time distribution function is thus given by $f_\alpha(y+x,t) \propto e^{ig_\alpha(y+x,t)}$ with the exponent (see the SM [58])

$$g_\alpha(y+x,t) = \int_{-\infty}^{+\infty} d\omega[e^{-i\omega t}-1]\frac{S^{\alpha\alpha}_{y+x}(\omega)}{\omega^2}. \quad (5)$$

The energy-dependent distribution function of the cold EC $f_-(y+x,E)$ is plotted in Fig. 3(b) in the limiting case $\varrho \to 0$. Different curves refer to different distribution functions: orange for the full-interacting case, purple without cross-correlations at x, i.e., $S^{\alpha\bar{\alpha}}_x(\omega)=0$. As a reference, we also plot the Fermi function evaluated with the same

effective temperature $T_{-}^{\rm eff}(y+x)$, see black-solid line in Fig. 3(b). The electron distribution differences are mainly due to the power-law behavior around $\mu = 0$ typical of a TL liquid. However, one immediately notes the nontrivial role of cross-correlations: they affect the electron distributions mainly at intermediate distances $y \sim x_K^+$. Indeed, at short distances the term $i\sin[\omega x(1-K)/v_F]$ suppresses their contribution. For long distances $y \gg x_K^+$, $f_-(y+x,E)$ with and without cross-correlations become equal, but still slightly different from the equilibrium Fermi distribution function. This is a consequence of the constraints dictated by integrability. However, the system spontaneously seems to develop a Fermi-like behavior even if it slightly differs from Fermi distribution at μ, a clear hallmark of the e-e interaction [31,61,62].

Thermoelectric currents. Equation (1) gives a direct way to detect the deviation of the cold EC (−) from the equilibrium distribution via the thermoelectric current. For this, we use a narrow-band spectrometer [61,62] such as a resonant antidot [63] with transmission $\mathcal{T}(E) \approx \Gamma\delta(E-E_r)$, which has the dual property of being an efficient thermoelectric [64] component sensitive to the features near the tunable resonant energy E_r, i.e., $I = -e\Gamma[f_{eq}(E_r,T_-) - f_-(x,E_r)]$, see Fig. 3(c). As expected the current increases with the length of the interaction distance $y+x$, since more energy is transferred between hot and cold ECs. Clearly, the thermocurrent saturates when $y \gg x_K^+$ (not shown).

The thermoelectric response also gives a DC measure of the effect of cross-correlations in the energy exchange by using the slightly more complex setup of Fig. 3(a). The interaction effects are measured by tuning QPC_1, which couples the outer channel to a probe terminal with a transmission probability λ. This way we can directly compare the thermoelectric current generated from the noninteracting Fermi distribution of the probe (λ=1) with the distribution coming from the interaction region (λ=0). This is represented by the difference of thermocurrents $\delta I_\lambda = I(\lambda{=}0) - I(\lambda{=}1)$. The comparison is particularly meaningful as the probe has the same temperature of the cold EC channel entering, i.e., $T_{+}^{\rm eff}(x+y)$ [65].

The effect of cross-correlations is detected by acting on QPC_2, which couples the upper and lower inner channels with transition probability κ. In this case, it is important to note that there are copies of terminals 2 and 3 that we call 2' and 3', which symmetrically operate on the ECs of the other side of the Hall bar. For $\kappa = 0$, the two upper channels interact along a distance $x+y$ as discussed above. Switching on the connection, $\kappa = 1$, one replaces the inner channel with another one having nominally the same auto- but no cross-correlations at x (as they could not interact before). The effect of cross-correlations in the thermocurrent is represented by the difference $\delta I_\kappa = I(\kappa{=}0) - I(\kappa{=}1)$.

Interaction and correlation effects. We firstly consider to control λ of the QPC_1 keeping fixed the QPC_2 ($\kappa = 0$). This is shown in Figs. 4(a) and 4(b) for different initial reservoir temperatures $\varrho = T_-/T_+$ varying the resonance energy E_r. A finite δI_λ means that the electronic distribution emerging from the interacting zone is different from a Fermi distribution. Thermoelectricity is sensitive to this difference, especially in the energy window around μ. The thermocurrent generally grows with the increasing temperature difference. Note that δI_λ is an odd function around $\mu = 0$ and it is maximal when

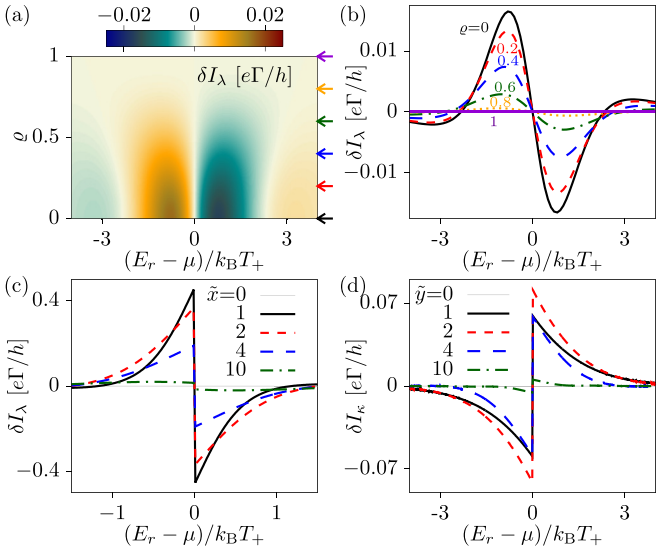

FIG. 4. (a) Difference of the currents with and without the probe, δI_λ, for $\tilde{x}$=300 with an antidot-like scatterer with $\mathcal{T}(E) = \Gamma\delta(E-E_r)$, as a function of the resonance energy $(E_r-\mu)/k_BT_+$ and ϱ. (b) Cuts of the previous for fixed values of ϱ marked by the corresponding color arrows in panel (a). (c) δI_λ for different values of $\tilde{x}$ and $\varrho = 10^{-3}$. (d) δI_κ when resetting cross-correlations at a distance $\tilde{x}$, measured after the distance $\tilde{y} = y/x_K^+$, for $\varrho = 10^{-3}$ and $\lambda = 0$.

$|E_r-\mu| \sim k_BT_+$, roughly the energy scale where the two-electron distributions are maximally different [66]. However, for the long interaction length limit $y+x \gg x_K^+$, the interacting electron distribution becomes Fermi like and δI_λ gets reduced, see Fig. 4(c).

If instead, we control κ of the QPC_2 keeping QPC_1 fixed at $\lambda = 0$, we can observe some intriguing effects for cross-correlations. In Fig. 4(d) we consider the case $x = x_K^+$ for different distances y, finding a nonmonotonous behavior in y. For $y \ll x_K^+$ the cross-correlations do not have enough space to develop an influence on the auto-correlations due to the sine prefactor of Eq. (4), so we expect $\delta I_\kappa \approx 0$. At the same time for $y \gg x_K^+$ we also expect $\delta I_\kappa \to 0$ because the resulting interacting electron distribution is Fermi like [see also Fig. 3(b)] and the cross-correlation does not play any major role in this limit. The role of the correlations in the energy flow between the two channels is maximal for $y \approx x_K^+$ and for $|E_r-\mu| \sim k_BT_+$, see Fig. 4(d). Using the realistic sub-Kelvin temperature gradients assumed before we expect a measurable DC current differences δI_i of the order of 0.1 nA.

Conclusions. We propose the nonlocal thermoelectric response as a signature of the presence of interacting nonequilibrium states in copropagating QH channels. We identify the characteristic length over which energy is exchanged due to the interaction, which manifests in the generated thermocurrent and gives a direct measure of the interaction strength. Controlling the connections between the different edge channels, the importance of cross-correlations in the energy flow of interacting nonequilibrium systems is quantified in a purely DC setup, opening ways to thermoelectricity-based quantum sensing. Our results introduce a circuit theory that can be extended to configurations with other kinds of edge states (e.g., in topological insulators), or with long-range interactions.

Acknowledgments. A.B. acknowledges the MUR-PRIN2022 Project NEThEQS (Grant No. 2022B9P8LN), the Royal Society through the International Exchanges between the UK and Italy (Grant No. IEC R2 192166) and EU's Horizon 2020 Research and Innovation Framework Programme under Grants No. 964398 (SUPERGATE) and No. 101057977 (SPECTRUM). M.C. acknowledges support from PRIN MUR Grant No. 2022PH852L. B.S. acknowledges financial support from the Ministry of Innovation NRW via the "Programm zur Förderung der Rückkehr des hochqualifizierten Forschungsnachwuchses aus dem Ausland" and Deutsche Forschungsgemeinschaft (DFG, German Research Foundation) - Project-ID 278162697 – SFB 1242. R.S. acknowledges funding from the Ramón y Cajal program RYC-2016-20778, and the Spanish Ministerio de Ciencia e Innovación via Grant No. PID2019-110125GB-I00 and through the "María de Maeztu" Programme for Units of Excellence in R&D CEX2018-000805-M, and the COST Action MP1209 short term scientific mission during which this project was initiated.

[1] G. Benenti, G. Casati, K. Saito, and R. S. Whitney, Fundamental aspects of steady-state conversion of heat to work at the nanoscale, Phys. Rep. **694**, 1 (2017).

[2] R. Sánchez, P. Burset, and A. L. Yeyati, Cooling by Cooper pair splitting, Phys. Rev. B **98**, 241414(R) (2018).

[3] R. Hussein, M. Governale, S. Kohler, W. Belzig, F. Giazotto, and A. Braggio, Nonlocal thermoelectricity in a Cooper-pair splitter, Phys. Rev. B **99**, 075429 (2019).

[4] Z. B. Tan, A. Laitinen, N. S. Kirsanov, A. Galda, V. M. Vinokur, M. Haque, A. Savin, D. S. Golubev, G. B. Lesovik, and P. J. Hakonen, Thermoelectric current in a graphene Cooper pair splitter, Nat. Commun. **12**, 138 (2021).

[5] S.-Y. Hwang, P. Burset, and B. Sothmann, Odd-frequency superconductivity revealed by thermopower, Phys. Rev. B **98**, 161408(R) (2018).

[6] N. R. Claughton and C. J. Lambert, Thermoelectric properties of mesoscopic superconductors, Phys. Rev. B **53**, 6605 (1996).

[7] G. Germanese, F. Paolucci, G. Marchegiani, A. Braggio, and F. Giazotto, Bipolar thermoelectric Josephson engine, Nat. Nanotechnol. **17**, 1084 (2022).

[8] R. Takahashi and S. Murakami, Thermoelectric transport in topological insulators, Semicond. Sci. Technol. **27**, 124005 (2012).

[9] F. Ronetti, L. Vannucci, G. Dolcetto, M. Carrega, and M. Sassetti, Spin-thermoelectric transport induced by interactions and spin-flip processes in two-dimensional topological insulators, Phys. Rev. B **93**, 165414 (2016).

[10] S. I. Erlingsson, A. Manolescu, G. A. Nemnes, J. H. Bardarson, and D. Sanchez, Reversal of thermoelectric current in tubular nanowires, Phys. Rev. Lett. **119**, 036804 (2017).

[11] N. Xu, Y. Xu, and J. Zhu, Topological insulators for thermoelectrics, npj Quantum Mater. **2**, 51 (2017).

[12] G. Blasi, F. Taddei, L. Arrachea, M. Carrega, and A. Braggio, Nonlocal thermoelectricity in a superconductor–topological-insulator–superconductor junction in contact with a normal-metal probe: Evidence for helical edge states, Phys. Rev. Lett. **124**, 227701 (2020).

[13] Y. Kleeorin, H. Thierschmann, H. Buhmann, A. Georges, L. W. Molenkamp, and Y. Meir, How to measure the entropy of a mesoscopic system via thermoelectric transport, Nat. Commun. **10**, 5801 (2019).

[14] A. Hijano, F. S. Bergeret, F. Giazotto, and A. Braggio, Microwave-assisted thermoelectricity in $S - I - S'$ tunnel junctions, Phys. Rev. Appl. **19**, 044024 (2023).

[15] G. Granger, J. P. Eisenstein, and J. L. Reno, Observation of chiral heat transport in the quantum Hall regime, Phys. Rev. Lett. **102**, 086803 (2009).

[16] S.-G. Nam, E. H. Hwang, and H.-J. Lee, Thermoelectric detection of chiral heat transport in graphene in the quantum Hall regime, Phys. Rev. Lett. **110**, 226801 (2013).

[17] R. Sánchez, B. Sothmann, and A. N. Jordan, Chiral thermoelectrics with quantum Hall edge states, Phys. Rev. Lett. **114**, 146801 (2015).

[18] D. L. Kovrizhin and J. T. Chalker, Equilibration of integer quantum Hall edge states, Phys. Rev. B **84**, 085105 (2011).

[19] S. M. Tabatabaei, D. Sánchez, A. L. Yeyati, and R. Sánchez, Nonlocal quantum heat engines made of hybrid superconducting devices, Phys. Rev. B **106**, 115419 (2022).

[20] H. Thierschmann, R. Sánchez, B. Sothmann, F. Arnold, C. Heyn, W. Hansen, H. Buhmann, and L. W. Molenkamp, Three-terminal energy harvester with coupled quantum dots, Nat. Nanotechnol. **10**, 854 (2015).

[21] G. Jaliel, R. K. Puddy, R. Sánchez, A. N. Jordan, B. Sothmann, I. Farrer, J. P. Griffiths, D. A. Ritchie, and C. G. Smith, Experimental realization of a quantum dot energy harvester, Phys. Rev. Lett. **123**, 117701 (2019).

[22] S. Dorsch, A. Svilans, M. Josefsson, B. Goldozian, M. Kumar, C. Thelander, A. Wacker, and A. Burke, Heat driven transport in serial double quantum dot devices, Nano Lett. **21**, 988 (2021).

[23] B. Karmakar, D. Venturelli, L. Chirolli, F. Taddei, V. Giovannetti, R. Fazio, S. Roddaro, G. Biasiol, L. Sorba, V. Pellegrini, and F. Beltram, Controlled coupling of spin-resolved quantum Hall edge states, Phys. Rev. Lett. **107**, 236804 (2011).

[24] T. Fujisawa, Nonequilibrium charge dynamics of Tomonaga–Luttinger liquids in quantum Hall edge channels, Ann. Phys. **534**, 2100354 (2022).

[25] I. P. Levkivskyi and E. V. Sukhorukov, Energy relaxation at quantum Hall edge, Phys. Rev. B **85**, 075309 (2012).

[26] T. Ota, S. Akiyama, M. Hashisaka, K. Muraki, and T. Fujisawa, Spectroscopic study on hot-electron transport in a quantum Hall edge channel, Phys. Rev. B **99**, 085310 (2019).

[27] S. Akiyama, T. Hirasawa, Y. Sato, T. Akiho, K. Muraki, and T. Fujisawa, Ballistic hot-electron transport in a quantum Hall edge channel defined by a double gate, Appl. Phys. Lett. **115**, 243106 (2019).

[28] E. Bocquillon, V. Freulon, J.-M. Berroir, P. Degiovanni, B. Plaçais, A. Cavanna, Y. Jin, and G. Fève, Separation of neutral and charge modes in one-dimensional chiral edge channels, Nat. Commun. **4**, 1839 (2013).

[29] K. Washio, R. Nakazawa, M. Hashisaka, K. Muraki, Y. Tokura, and T. Fujisawa, Long-lived binary tunneling spectrum in the quantum Hall Tomonaga-Luttinger liquid, Phys. Rev. B **93**, 075304 (2016).

[30] M. Hashisaka, N. Hiyama, T. Akiho, K. Muraki, and T. Fujisawa, Waveform measurement of charge- and spin-density wavepackets in a chiral Tomonaga–Luttinger liquid, Nat. Phys. **13**, 559 (2017).

[31] K. Itoh, R. Nakazawa, T. Ota, M. Hashisaka, K. Muraki, and T. Fujisawa, Signatures of a nonthermal metastable state in copropagating quantum Hall edge channels, Phys. Rev. Lett. **120**, 197701 (2018).

[32] R. H. Rodriguez, F. D. Parmentier, D. Ferraro, P. Roulleau, U. Gennser, A. Cavanna, M. Sassetti, F. Portier, D. Mailly, and P. Roche, Relaxation and revival of quasiparticles injected in an interacting quantum Hall liquid, Nat. Commun. **11**, 2426 (2020).

[33] K. Suzuki, T. Hata, Y. Sato, T. Akiho, K. Muraki, and T. Fujisawa, Non-thermal Tomonaga-Luttinger liquid eventually emerging from hot electrons in the quantum Hall regime, Commun. Phys. **6**, 103 (2023).

[34] R. Konuma, C. Lin, T. Hata, T. Hirasawa, T. Akiho, K. Muraki, and T. Fujisawa, Nonuniform heat redistribution among multiple channels in the integer quantum Hall regime, Phys. Rev. B **105**, 235302 (2022).

[35] P. Degiovanni, C. Grenier, and G. Fève, Decoherence and relaxation of single-electron excitations in quantum Hall edge channels, Phys. Rev. B **80**, 241307(R) (2009).

[36] P. Degiovanni, C. Grenier, G. Fève, C. Altimiras, H. le Sueur, and F. Pierre, Plasmon scattering approach to energy exchange and high-frequency noise in $\nu = 2$ quantum Hall edge channels, Phys. Rev. B **81**, 121302(R) (2010).

[37] S. G. Fischer, Y. Meir, Y. Gefen, and B. Rosenow, Near-frozen nonequilibrium state at high energy in an integrable system, Phys. Rev. B **108**, L081121 (2023).

[38] S. Jezouin, F. D. Parmentier, A. Anthore, U. Gennser, A. Cavanna, Y. Jin, and F. Pierre, Quantum limit of heat flow across a single electronic channel, Science **342**, 601 (2013).

[39] C. L. Kane and M. P. A. Fisher, Quantized thermal transport in the fractional quantum Hall effect, Phys. Rev. B **55**, 15832 (1997).

[40] M. Banerjee, M. Heiblum, V. Umansky, D. E. Feldman, Y. Oreg, and A. Stern, Observation of half-integer thermal Hall conductance, Nature (London) **559**, 205 (2018).

[41] K. K. W. Ma and D. E. Feldman, Partial equilibration of integer and fractional edge channels in the thermal quantum Hall effect, Phys. Rev. B **99**, 085309 (2019).

[42] G. Le Breton, R. Delagrange, Y. Hong, M. Garg, K. Watanabe, T. Taniguchi, R. Ribeiro-Palau, P. Roulleau, P. Roche, and F. D. Parmentier, Heat equilibration of integer and fractional quantum Hall edge modes in graphene, Phys. Rev. Lett. **129**, 116803 (2022).

[43] B. Dutta, W. Yang, R. Melcer, H. K. Kundu, M. Heiblum, V. Umansky, Y. Oreg, A. Stern, and D. Mross, Distinguishing between non-Abelian topological orders in a quantum Hall system, Science **375**, 193 (2022).

[44] R. A. Melcer, B. Dutta, C. Spånslätt, J. Park, A. D. Mirlin, and V. Umansky, Absent thermal equilibration on fractional quantum Hall edges over macroscopic scale, Nat. Commun. **13**, 376 (2022).

[45] S. K. Srivastav, R. Kumar, C. Spånslätt, K. Watanabe, T. Taniguchi, A. D. Mirlin, Y. Gefen, and A. Das, Vanishing thermal equilibration for hole-conjugate fractional quantum Hall states in graphene, Phys. Rev. Lett. **126**, 216803 (2021).

[46] A. Marguerite, J. Birkbeck, A. Aharon-Steinberg, D. Halbertal, K. Bagani, I. Marcus, Y. Myasoedov, A. K. Geim, D. J. Perello, and E. Zeldov, Imaging work and dissipation in the quantum Hall state in graphene, Nature (London) **575**, 628 (2019).

[47] J. N. Moore, A. Kamiyama, T. Mano, and G. Yusa, Thermal transport imaging in the quantum Hall edge channel, Europhys. Lett. **142**, 16004 (2023).

[48] R. Sánchez and M. Büttiker, Optimal energy quanta to current conversion, Phys. Rev. B **83**, 085428 (2011).

[49] We are neglecting direct electron tunnelling between the two channels since we assume the equilibration length between the two channels longer than the sample size, and disorder-induced equilibration processes, which are expected for length scales $\gtrsim 10\mu$m.

[50] U. Sivan and Y. Imry, Multichannel Landauer formula for thermoelectric transport with application to thermopower near the mobility edge, Phys. Rev. B **33**, 551 (1986).

[51] P. N. Butcher, Thermal and electrical transport formalism for electronic microstructures with many terminals, J. Phys.: Condens. Matter **2**, 4869 (1990).

[52] S.-i. Tomonaga, Remarks on Bloch's method of sound waves applied to many-fermion problems, Prog. Theor. Phys. **5**, 544 (1950).

[53] J. M. Luttinger, An exactly soluble model of a many-fermion system, J. Math. Phys. **4**, 1154 (1963).

[54] F. D. M. Haldane, 'Luttinger liquid theory' of one-dimensional quantum fluids. I. Properties of the Luttinger model and their extension to the general 1D interacting spinless Fermi gas, J. Phys. C: Solid State Phys. **14**, 2585 (1981).

[55] J. von Delft and H. Schoeller, Bosonization for beginners—refermionization for experts, Ann. Phys. **510**, 225 (1998).

[56] A. Braggio, D. Ferraro, M. Carrega, N. Magnoli, and M. Sassetti, Environmental induced renormalization effects in quantum Hall edge states due to $1/f$ noise and dissipation, New J. Phys. **14**, 093032 (2012).

[57] M. Acciai, M. Carrega, J. Rech, T. Jonckheere, T. Martin, and M. Sassetti, Probing interactions via nonequilibrium momentum distribution and noise in integer quantum Hall systems at $\nu = 2$, Phys. Rev. B **98**, 035426 (2018).

[58] See Supplemental Material at http://link.aps.org/supplemental/10.1103/PhysRevResearch.6.L012049 for detailed computations of noise spectral densities, the thermal currents, the heat conductance universal laws, and the electron distributions in different limits, which includes Ref. [67].

[59] G. Blasi, G. Haack, V. Giovannetti, F. Taddei, and A. Braggio, Topological Josephson junctions in the integer quantum Hall regime, Phys. Rev. Res. **5**, 033142 (2023).

[60] The cross-correlations emerge due to the interaction along the distance x for an open QPC_2 ($\kappa = 1$) but, when closed ($\kappa = 0$) the two ECs come from different circuits, which avoids cross-correlations.

[61] C. Altimiras, H. le Sueur, U. Gennser, A. Cavanna, D. Mailly, and F. Pierre, Non-equilibrium edge-channel spectroscopy in the integer quantum Hall regime, Nat. Phys. **6**, 34 (2010).

[62] H. le Sueur, C. Altimiras, U. Gennser, A. Cavanna, D. Mailly, and F. Pierre, Energy relaxation in the integer quantum Hall regime, Phys. Rev. Lett. **105**, 056803 (2010).

[63] M. Büttiker, Negative resistance fluctuations at resistance minima in narrow quantum Hall conductors, Phys. Rev. B **38**, 12724 (1988).

[64] M. Josefsson, A. Svilans, A. M. Burke, E. A. Hoffmann, S. Fahlvik, C. Thelander, M. Leijnse, and H. Linke, A quantum-dot heat engine operating close to the thermodynamic efficiency limits, Nat. Nanotechnol. **13**, 920 (2018).

[65] J. Meair, J. P. Bergfield, C. A. Stafford, and P. Jacquod, Local temperature of out-of-equilibrium quantum electron systems, Phys. Rev. B **90**, 035407 (2014).

[66] This means that the narrow-resonance assumption can be even relaxed up to $\Gamma \sim k_B T_+$ resulting in larger thermocurrent [58].

[67] M. Büttiker, Coherent and sequential tunneling in series barriers, IBM J. Res. Dev. **32**, 63 (1988).